Front. Optoelectron. 2012, 5(3): 248–255
DOI 10.1007/s12200-012-0267-9

REVIEW ARTICLE

Polarization properties in helical metamaterials

Zhenyu YANG (✉)[1], Peng ZHANG[1], Peiyuan XIE[2], Lin WU[1], Zeqin LU[1], Ming ZHAO[1]

1 Wuhan National Laboratory for Optoelectronics, College of Optoelectronic Science and Engineering, Huazhong University of Science and Technology, Wuhan 430074, China
2 Hunan Electric Power Company Dispatches & Communication Center, Changsha 410007, China

Abstract In the last few years, there has been growing interest in the research of helical metamaterials due to the advantages of giant circular dichroism, broad operation bands, and compact structures. However, most of the researches were in the cases of single-, circular-helical metamaterials, and normal incidences. In this paper, we reviewed recent simulation works in the helical metamaterials with the finite-difference time-domain (FDTD) method, which mainly included the optical performances of double-, three-, four-helical metamaterials, performances of elliptical-helical metamaterials, and the polarization properties under the condition of oblique incidences. The results demonstrate that the double-helical metamaterials have operation bands more than 50%, which is broader than those of the single-helical structures. But both of them have low signal-to-noise ratios about 10 dB. The three- and four-helical metamaterials have significant improvement in overall performance. For elliptical-helixes, simulation results suggest that the transmitted light can have elliptical polarization states. On the condition of oblique incidences, the novel property of tunable polarization states occurred in the helical metamaterials, which could have much broader potential applications such as tunable optical polarizers, tunable beam splitters, and tunable optical attenuators.

Keywords finite-difference time-domain (FDTD) method, polarization, chiral media, helical metamaterials

1 Introduction

Metamaterials, which are engineered composite media, can be designed and constructed to exhibit unconventional characteristics and new response functions for the constitutive parameters. In the last decade, there has been growing interest in the study of the metamaterials in the research community both theoretically and experimentally due to their exciting potential applications ranging from perfect lenses [1], cloaking devices [2–4] and slow lights [5] to sub-wavelength optical waveguides [6,7], ultra-sensitive sensors [8–10], microstructured magnetic materials [11,12] and circular dichroism [13–16]. Recently, Gansel et al. [17–19] have succeeded in developing a broadband circular polarizer using gold single-helical metamaterials; Wu et al. studied metallic helix arrays theoretically and experimentally in microwave ranges [20,21].

Circular polarization of light is attractive for applications in reflective color displays [22–24], life science microscopy, and photography [25,26]. Generally, there are two ways of obtaining circular polarized light: one is using a linear polarizer and a quarter-wave plate [27], which is the most common method in optics; the other is utilizing cholesteric liquid crystals (CLC) [28–31], which are self-assembled photonic crystals formed by rod-like molecules. Compared with these two methods, the helical metamaterials has advantages of broad wavelength ranges and compact structures, which are convenient to be integrated with other optical devices.

As far as we know, however, most of the researches on the helical metamaterials were under the cases of single-, circular-helixes, and normal incidences. In this paper, recent simulation works by the finite difference time domain (FDTD) method on the helical metamaterials are reviewed, which mainly included the optical performances of double-, three-, four-helical metamaterials, performances of the elliptical-helical metamaterials, and the polarization properties under the condition of oblique incidences [32–36]. The results demonstrate that the double-helical metamaterials has operation bands more than 50% broader than the single-helical structures.

Received May 3, 2012; accepted June 1, 2012

E-mail: zyang@mail.hust.edu.cn

But both of them have low signal-to-noise ratios about 10 dB. The three- and four-helical metamaterials have a significant improvement in overall performance. For elliptical-helixes, simulation results showed that the output light can have elliptical polarization states. On the condition of oblique incidences, a novel property of tunable polarization states occurred in the helical metamaterials, which could have much broader potential applications such as tunable optical polarizers, tunable beam splitters, and tunable optical attenuators.

2 Simulation models

Figure 1 shows the schematic diagrams of a single-helical metamaterials. It consists of left-handed helical nanowire arrays and a substrate of silica. In Fig. 1, DW, NH, SG, LH, and DH stand for the diameter of the wire, the number of the helix-periods, the spacing of the grid, the length of the helix-period, and the diameter of the helix, respectively. Two kinds of polarized lights, left-handed circularly polarized (LCP) and right-handed circularly polarized (RCP) lights are used as the excitation sources to irradiate the metamaterials along the Z direction, respectively. To simplify the simulation, a broadband Gaussian-modulated pulsed light source is used as the excitation source. The perfectly matched layers (PMLs) [37] were used as the boundary conditions. The boundaries along X and Y directions were confined with the periodic boundary conditions [38], due to the periodicity of the nanowire metamaterials. During the calculation, the dielectric function of the metals was described by the Lorentz-Drude model [39].

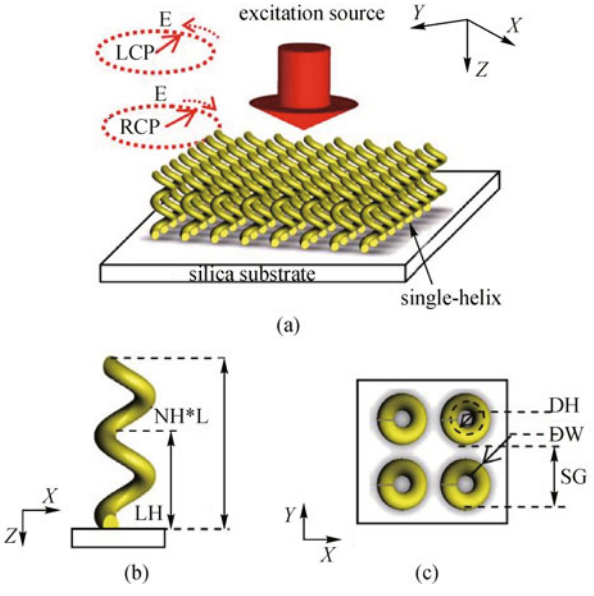

Fig. 1 Schematic diagrams of single-helical metamaterials

3 Simulation results and analyses

3.1 Double-helical metamaterials

Single- and double-helical metamaterials with two different metals, gold (Au) and aluminum (Al) were simulated using the FDTD method. Figure 2 shows the schematic diagram of a double-helical metamaterials. The parameters of the metamaterial structure are: DW = 50 nm, NH = 3, SG = 190 nm, LH = 200 nm, and DH = 100 nm, respectively. Their optical performances are shown in Fig. 3. Figures 3(a) and 3(c) are transmittances of the circular polarizers for the LCP and RCP light beams and the extinction ratio as functions of the wavelength for the single-helical structure of Au and Al nanowires, respectively. Figures 3(b) and 3(d) are the results for the double-helical structure of Au and Al nanowires, respectively.

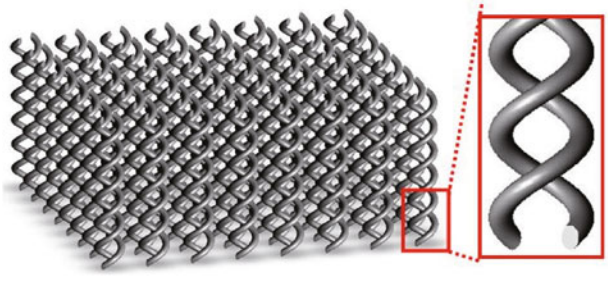

Fig. 2 Schematic diagrams of double-helical metamaterials

The operation regions of the circular polarizers are defined as the wavelength regions, in which the extinction ratio is not less than 1/e of its peak value. In the operation regions, the average transmittances for the RCP light and the average extinction ratios with respect to single- and double- helix metamaterials and different metals are shown in Fig. 3 and listed in Table 1. It is very clear that the operation regions of the circular polarizers with the double-helical structures are more than 50% broader than those of the single-helical structures.

The mechanism may be come from the coupling effect in metamaterials. In a general model of metamaterial, one single-helix can be seen as an artificial atom. The double-helix structure can be seen as molecule composed from two coupled helix atoms. For two coupled helix resonators, the mode can be seen as hybridized mode from single-helix resonator. Hybridization usually results broadening of spectrum of resonance mode. Then it may give an explanation why the double-helix has much broader band than the single-helix [40,41].

3.2 Three- and four-helical metamaterials

The single-, double-, three-, and four-helical Al metamaterials were simulated using the FDTD method. Figures

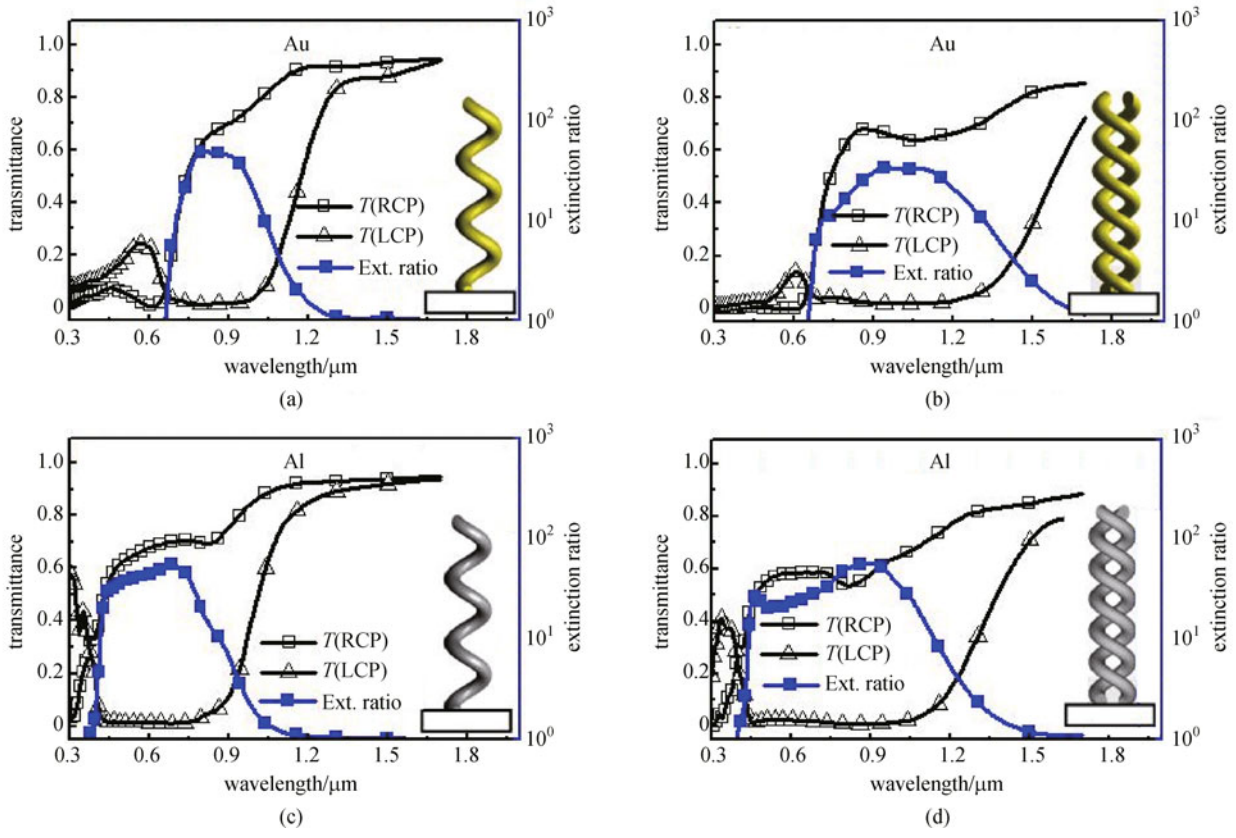

Fig. 3 Comparison of optical performances between single- and double-helical metamaterials. (a) and (b) Au single- and double-helix; (c) and (d) Al single- and double-helix

Table 1 Comparison of optical performances between single- and double-helical metamaterials

		operation regions/μm	average transmittances of RCP light/%	average extinction ratios
Au	single-helix	0.72–1.00	63	36:1
	double-helix	0.75–1.30	65	25:1
Al	single-helix	0.42–0.79	63	39:1
	double-helix	0.44–1.10	56	31:1

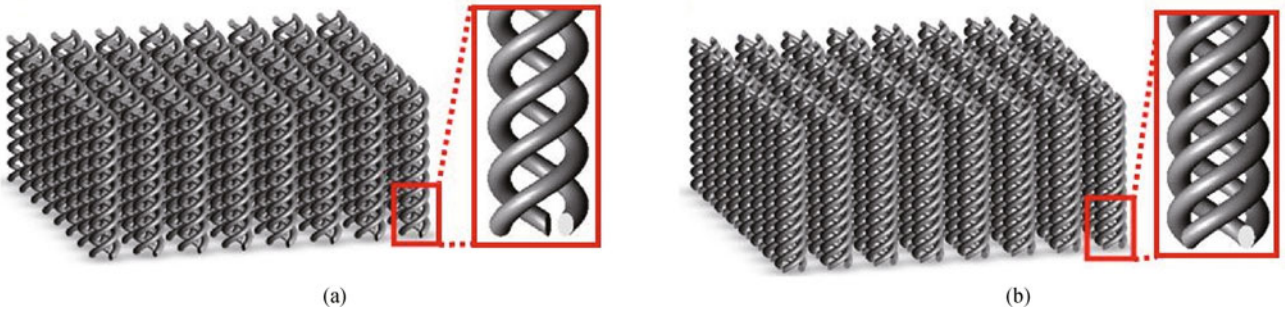

Fig. 4 Schematic diagrams of (a) three- and (b) four-helical metamaterials

4(a) and 4(b) show the schematic diagrams of the three- and four-helix, respectively. The optical performances of the incident and transmitted lightwaves are shown in Fig. 5. Figure 5(a) shows schematic diagram of the amplitude (Amp.) and the phase angle (θ) of the electric vector; Fig. 5(b) shows the amplitude and the phase angle for the

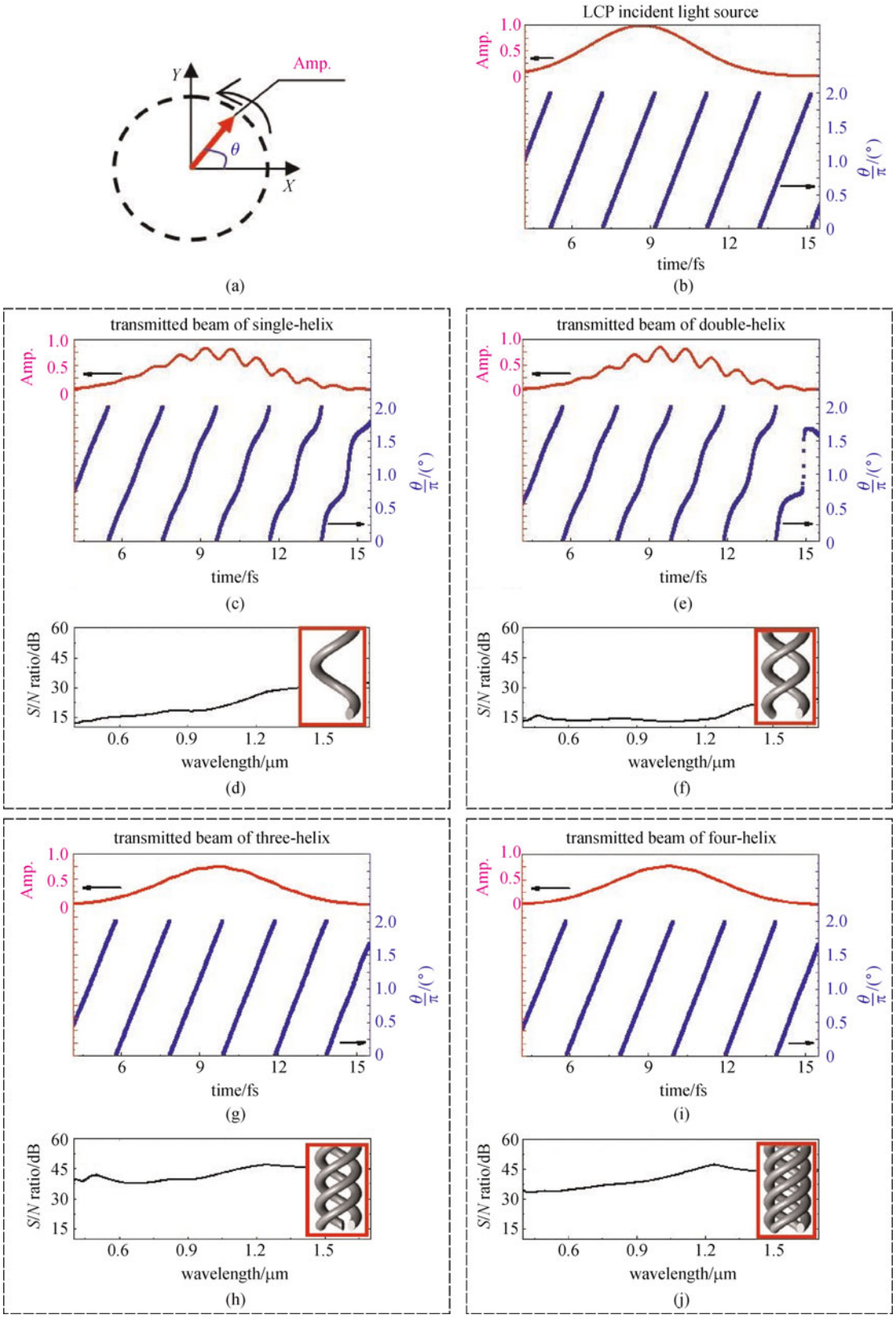

Fig. 5 Optical performances of LCP incident light, and transmitted lights through single-, double-, three-, and four-helix

LCP incident light; Figs. 5(c), 5(e), 5(g), and 5(i) are the results for the transmitted lights through the single-, double-, three-, and four-helical structures, respectively; Figs. 5(d), 5(f), 5(h), and 5(j) are the *S*/*N* ratios for them, respectively. From the simulation results, it is very clear that the *S*/*N* ratios of the three- and four-helixes are two orders higher than those of single- and double-helical ones.

3.3 Elliptical-helical metamaterials

Figure 6 shows the schematic diagram of the elliptically single-helical metamaterials, in which LEH, SHE, SGL, and SGS stand for long-axis of elliptical helix, short-axis of elliptical helix, and spacing of grids in long-axis direction and in short-axis direction, respectively. The axial ratio (the length of the major semiaxis to that of the minor semiaxis) is 2∶1. The metal is Al. The excitation sources are orthogonal left-elliptically polarized (LEP) light and right-elliptically polarized (REP) light propagating along *Z* axis in free space. They are represented with the following Jones vectors [20]:

$$\text{LEP}: \frac{1}{\sqrt{5}}\begin{bmatrix} 1 \\ -2\text{i} \end{bmatrix}, \quad \text{REP}: \frac{1}{\sqrt{5}}\begin{bmatrix} 2 \\ \text{i} \end{bmatrix}.$$

The parameters' values are: DW = 30 nm, NH = 3, LH = 200 nm, LEH = 80 nm, SEH = 40 nm, SGL = 310 nm, and SGS = 170 nm. Figure 6(a) shows the transmittance and the extinction ratio of the structure, in which the operation region is 680–1100 nm. In the region, the average transmittance of LEP light is 74% and the average extinction ratio is 11.1 dB. It is obvious that this metamaterials has a giant elliptical dichroism. To analyze the polarization states of the transmitted LEP light in detail, the Poincaré sphere [42] is plotted in Fig. 6(b), in which these red points refer to different wavelengths. The coordinates of the points on the Poincaré sphere, their corresponding polarization states and the conversions of LEP are listed in Table 2. From the calculation results, it is clear that the axial ratios of the transmitted LEP light are all around 2∶1, which is the same as that of the incident LEP light.

3.4 Performances with oblique incidences

The helical metamaterials with different incident angles were simulated using the FDTD method. The parameters and the simulation results including the axial ratios, the extinction ratio, and the transmittances of LCP light are summarized in Table 3 and shown in Fig. 7. Figures 7(a)–

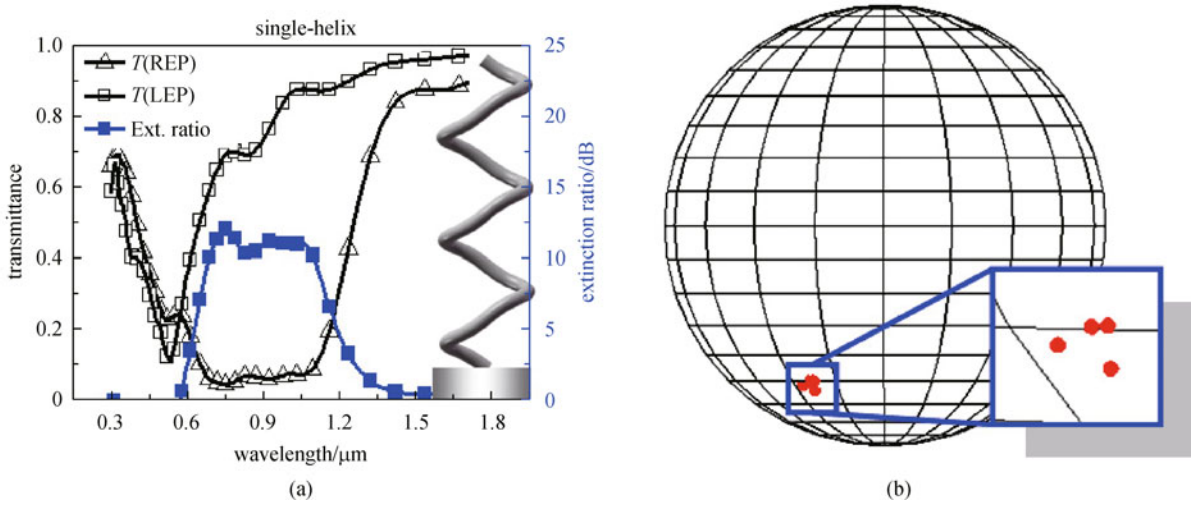

Fig. 6 (a) Optical performance of elliptically single-helical metamaterials; (b) polarization state of transmitted LEP light represented on Poincaré sphere

Table 2 Polarization states of transmitted LEP light

WL/m	coordinates	AR	conversion of LEP
1.07	(~0.58, 0.36,~0.72)	1.95	4.1%
0.93	(~0.63, 0.31,~0.70)	2.12	3.6%
0.83	(~0.62, 0.33,~0.70)	2.09	4.4%
0.75	(~0.58, 0.31,~0.74)	1.95	3.6%

WL: Wavelength, AR: axial ratio

Table 3 Parameters and simulation results with different incident angles

angle of incidence/(°)	axial ratio	transmittances of LCP light/%	extinction ratio	diagrams
20	1:0.93	57	5.04:1	Fig. 7(a), "●" in Fig. 7(f)
10	1:0.80	65	6.78:1	Fig. 7(b), "●" in Fig. 7(f)
0	1:0.67	69	7.58:1	Fig. 7(c), "●" in Fig. 7(f)
−10	1:0.66	68	7.71:1	Fig. 7(d), "●" in Fig. 7(f)
−20	1:0.59	62	6.22:1	Fig. 7(e), "●" in Fig. 7(f)

DW = 30 nm, NH = 3, SG = 200 nm, LH = 200 nm, DH = 100 nm

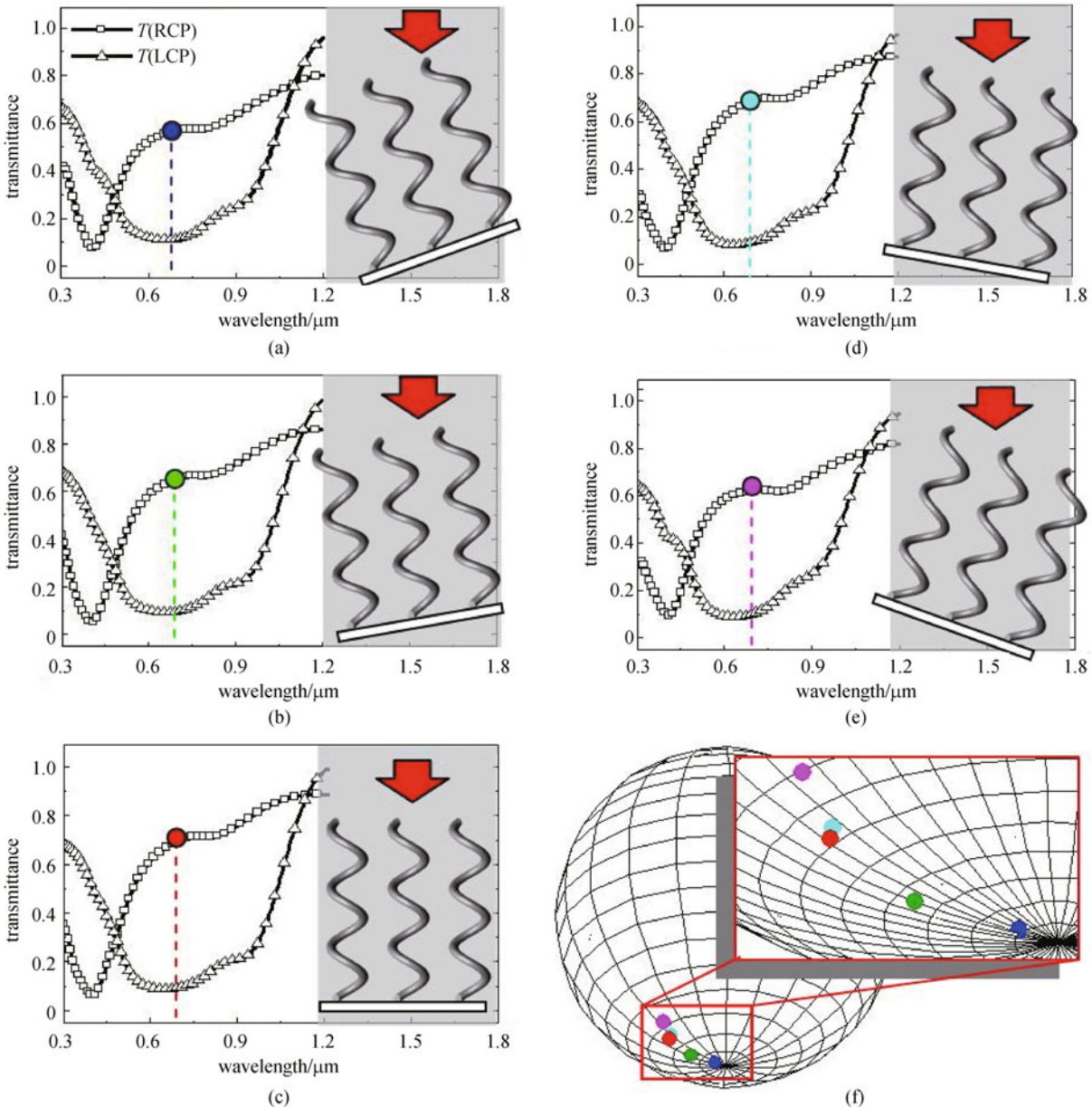

Fig. 7 Optical performances of the helical metamaterials with different incident angles. (a)–(e) are for the incident angles of 20°, 10°, 0°, –10°, and –20°, respectively; (f) is comparison of the transmitted light's polarization states (represented on the Poincaré sphere). The blue, green, red, cyan, and pink points refer to the incident angles of 20°, 10°, 0°, –10°, and –20°, respectively

7(e) are transmittances of the helical metamaterials with different incident angles 20°, 10°, 0°, −10°, and −20°, respectively. In Fig. 7(f), the Poincaré sphere was used to analyze the polarization states of the transmitted lights at wavelength 0.68 μm. Different color points refer to different incident angles. The closer the points are to the pole, the closer the axial ratios are to the value of 1∶1. From these simulation results, it is clear that the transmitted light has tunable polarization states with changing the incident angles.

4 Conclusions

In summary, this paper reviewed recent simulation works in the helical metamaterials, which mainly included the optical performances of double-, three-, four-helical metamaterials, performances of the elliptical-helical metamaterials, and the polarization properties under the condition of oblique incidences. The results demonstrate that the double-helical metamaterials has operation bands more than 50% broader than the single-helical structures. But both of them have low signal-to-noise ratios about 10 dB. The three- and four-helical metamaterials have a significant improvement in overall performance. For elliptical-helixes, simulation results show that the output light can have elliptical polarization states. On the condition of oblique incidences, a novel property of tunable polarization states occurred in the helical metamaterials, which could have much broader potential applications such as tunable optical polarizers, tunable beam splitters, and tunable optical attenuators.

It is certain that there are still some challenges on the fabrication of the real 3D helical metamaterials. In our opinions, two aspects of the helical metamaterials will become the development directions. One is improvements of nanofabrication techniques; the other is design of simple 2D chiral metamaterials, which also has circular dichroism, but need not complex fabrication processes. In a word, with developments of the metamaterials, more and more novel structures and devices could be realized in the near future.

Acknowledgements We acknowledge support by the Natural Natural Science Foundation of China (NSFC) (Grant Nos. 11104094, and 61007019), the Fundamental Research Funds for the Central Universities (HUST, Nos. 2010MS063 and 2011TS060), and the Fok Ying Tung Education Foundation (No. 132034).

References

1. Pendry J B. Negative refraction makes a perfect lens. Physical Review Letters, 2000, 85(18): 3966–3969
2. Alù A, Engheta N. Achieving transparency with plasmonic and metamaterial coatings. Physical Review E: Statistical, Nonlinear, and Soft Matter Physics, 2005, 72(1Pt2): 016623
3. Leonhardt U. Optical conformal mapping. Science, 2006, 312 (5781): 1777–1780
4. Pendry J B, Schurig D, Smith D R. Controlling electromagnetic fields. Science, 2006, 312(5781): 1780–1782
5. Monat C, Grillet C, Corcoran B, Moss D J, Eggleton B J, White T P, Krauss T F. Investigation of phase matching for third-harmonic generation in silicon slow light photonic crystal waveguides using Fourier optics. Optics Express, 2010, 18(7): 6831–6840
6. Alu A, Engheta N. Guided modes in a waveguide filled with a pair of singlenegative (SNG) double-negative (DNG), and/or double-positive (DPS) layers. IEEE Transactions on Microwave Theory and Techniques, 2004, 52(1): 199–210
7. Ma Y, Li X, Yu H, Tong L, Gu Y, Gong Q. Direct measurement of propagation losses in silver nanowires. Optics Letters, 2010, 35(8): 1160–1162
8. Wang P, Gu F, Zhang L, Tong L. Polymer microfiber rings for high-sensitivity optical humidity sensing. Applied Optics, 2011, 50(31): G7–G10
9. Meng C, Xiao Y, Wang P, Zhang L, Liu Y, Tong L. Quantum-dot-doped polymer nanofibers for optical sensing. Advanced Materials (Deerfield Beach, Fla.), 2011, 23(33): 3770–3774
10. Wu D K C, Kuhlmey B T, Eggleton B J. Ultrasensitive photonic crystal fiber refractive index sensor. Optics Letters, 2009, 34(3): 322–324
11. Wiltshire M C K, Pendry J B, Young I R, Larkman D J, Gilderdale D J, Hajnal J V. Microstructured magnetic materials for RF flux guides in magnetic resonance imaging. Science, 2001, 291(5505): 849–851
12. Wang X, Venugopal G, Zeng J, Chen Y, Lee D H, Litchinitser N M, Cartwright A N. Optical fiber metamagnetics. Optics Express, 2011, 19(21): 19813–19821
13. Liu H, Cao J X,.Zhu N, Liu N, Ameling R, Giessen H. Lagrange model for the chiral optical properties of stereometamaterials. Physical Review B: Condensed Matter and Materials Physics, 2010, 81(24): 241403
14. Li T Q, Liu H, Li T, Wang S M, Wang F M, Wu R X, Chen P, Zhu S N, Zhang X. Magnetic resonance hybridization and optical activity of microwaves in a chiral metamaterial. Applied Physics Letters, 2008, 92(13): 131111
15. Liu N, Liu H, Zhu S N, Giessen H. Stereometamaterials. Nature Photonics, 2009, 3: 157–162
16. Liu H, Genov D A, Wu D M, Liu Y M, Liu Z W, Sun C, Zhu S N, Zhang X. Magnetic plasmon hybridization and optical activity at optical frequencies in metallic nanostructures. Physical Review B: Condensed Matter and Materials Physics, 2007, 76(7): 073101
17. Gansel J K, Thiel M, Rill M S, Decker M, Bade K, Saile V, von Freymann G, Linden S, Wegener M. Gold helix photonic metamaterial as broadband circular polarizer. Science, 2009, 325 (5947): 1513–1515
18. Gansel J K, Wegener M, Burger S, Linden S. Gold helix photonic metamaterials: a numerical parameter study. Optics Express, 2010, 18(2): 1059–1069
19. Gansel J K, Latzel M, Frölich A, Kaschke J, Thiel M, Wegener M. Tapered gold-helix metamaterials as improved circular polarizers. Applied Physics Letters, 2012, 100(10): 101109

20. Wu C, Li H Q, Wei Z Y, Yu X T, Chan C T. Theory and experimental realization of negative refraction in a metallic helix array. Physical Review Letters, 2010, 105(24): 247401
21. Wu C, Li H Q, Yu X, Li F, Chen H. Metallic helix array as a broadband wave plate. Physical Review Letters, 2011, 107(17): 177401
22. Lub J, van de Witte P, Doornkamp C, Vogels J P A, Wegh R T. Stable photopatterned cholesteric layers made by photoisomerization and subsequent photopolymerization for use as color filters in liquid-crystal displays. Advanced Materials (Deerfield Beach, Fla.), 2003, 15(17): 1420–1425
23. De Filpo G, Nicoletta F P, Chidichimo G. Cholesteric emulsions for colored displays. Advanced Materials (Deerfield Beach, Fla.), 2005, 17(9): 1150–1152
24. Yoshioka T, Ogata T, Nonaka T, Moritsugu M, Kim S N, Kurihara S. Reversible-photon-mode full-color display by means of photochemical modulation of a helically cholesteric structure. Advanced Materials (Deerfield Beach, Fla.), 2005, 17(10): 1226–1229
25. Loksztejn A, Dzwolak W. Vortex-induced formation of insulin amyloid superstructures probed by time-lapse atomic force microscopy and circular dichroism spectroscopy. Journal of Molecular Biology, 2010, 395(3): 643–655
26. Claborn K, Puklin-Faucher E, Kurimoto M, Kaminsky W, Kahr B. Circular dichroism imaging microscopy: application to enantiomorphous twinning in biaxial crystals of 1,8-dihydroxyanthraquinone. Journal of the American Chemical Society, 2003, 125(48): 14825–14831
27. Hecht E. Optics. 4th ed. San Francisco: Addison-Wesley, 2002, 357–358
28. Hikmet R A M, Kemperman H. Electrically switchable mirrors and optical components made from liquid-crystal gels. Nature, 1998, 392(6675): 476–479
29. Mitov M, Dessaud N. Going beyond the reflectance limit of cholesteric liquid crystals. Nature Materials, 2006, 5(5): 361–364
30. Xiao J M, Cao H, He W L, Ma Z, Geng J, Wang L, Wang G, Yang H. Wide-band reflective polarizers from cholesteric liquid crystals with stable optical properties. Journal of Applied Polymer Science, 2007, 105(5): 2973–2977
31. Ha N Y, Ohtsuka Y, Jeong S M, Nishimura S, Suzaki G, Takanishi Y, Ishikawa K, Takezoe H. Fabrication of a simultaneous red-green-blue reflector using single-pitched cholesteric liquid crystals. Nature Materials, 2008, 7(1): 43–47
32. Yang Z Y, Zhao M, Lu Y F. Similar structures, different characteristics: optical performances of circular polarizers with single- and double-helical metamaterials. Journal of Lightwave Technology, 2010, 28(21): 3055–3061
33. Yang Z Y, Zhao M, Lu P X, Lu Y F. Ultrabroadband optical circular polarizers consisting of double-helical nanowire structures. Optics Letters, 2010, 35(15): 2588–2590
34. Yang Z Y, Zhao M, Lu P X. How to improve the signal-to-noise ratio for circular polarizers consisting of helical metamaterials? Optics Express, 2011, 19(5): 4255–4260
35. Wu L, Yang Z, Zhao M, Yu Y, Li S, Zhang Q, Yuan X. Polarization characteristics of the metallic structure with elliptically helical metamaterials. Optics Express, 2011, 19(18): 17539–17545
36. Wu L, Yang Z, Zhao M, Zhang P, Lu Z, Yu Y, Li S, Yuan X. What makes single-helical metamaterials generate “pure” circularly polarized light? Optics Express, 2012, 20(2): 1552–1560
37. Berenger J P. A perfectly matched layer for the absorption of electromagnetic-waves. Journal of Computational Physics, 1994, 114(2): 185–200
38. Harms P, Mittra R, Ko W. Implementation of the periodic boundary condition in the finite-difference time-domain algorithm for FSS structures. IEEE Transactions on Antennas and Propagation, 1994, 42(9): 1317–1324
39. Rakic A D, Djurisic A B, Elazar J M, Majewski M L. Optical properties of metallic films for vertical-cavity optoelectronic devices. Applied Optics, 1998, 37(22): 5271–5283
40. Liu H, Liu Y M, Li T, Wang S M, Zhu S N, Zhang X. Coupled magnetic plasmons in metamaterials. Physica Status Solidi B, 2009, 246(7): 1397–1406
41. Liu H, Li T, Wang S M, Zhu S N. Hybridization effect in coupled metamaterials. Frontiers of Physics in China, 2010, 5(3): 277–290
42. Rukhlenko I D, Dissanayake C, Premaratne M. Visualization of electromagnetic-wave polarization evolution using the Poincaré sphere. Optics Letters, 2010, 35(13): 2221–2223